ACS APPLIED MATERIALS & INTERFACES

Research Article

www.acsami.org

TiC/NiO Core/Shell Nanoarchitecture with Battery-Capacitive Synchronous Lithium Storage for High-Performance Lithium-Ion Battery

Hui Huang, Tong Feng, Yongping Gan, Mingyu Fang, Yang Xia, Chu Liang, Xinyong Tao,* and Wenkui Zhang*

College of Materials Science and Engineering, Zhejiang University of Technology, Hangzhou 310014, P. R. China

Supporting Information

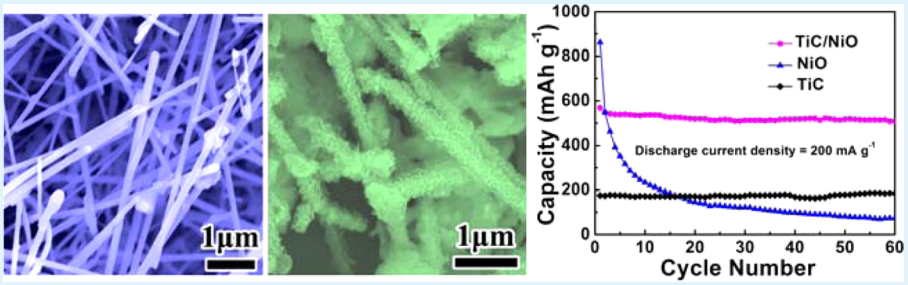

ABSTRACT: The further development of electrode materials with high capacity and excellent rate capability presents a great challenge for advanced lithium-ion batteries. Herein, we demonstrate a battery-capacitive synchronous lithium storage mechanism based on a scrupulous design of TiC/NiO core/shell nanoarchitecture, in which the TiC nanowire core exhibits a typical double-layer capacitive behavior, and the NiO nanosheet shell acts as active materials for Li^+ storage. The as-constructed TiC/NiO (32 wt % NiO) core/shell nanoarchitecture offers high overall capacity and excellent cycling ability, retaining above 507.5 mAh g^{-1} throughout 60 cycles at a current density of 200 mA g^{-1} (much higher than theoretical value of the TiC/NiO composite). Most importantly, the high rate capability is far superior to that of NiO or other metal oxide electrode materials, owing to its double-layer capacitive characteristics of TiC nanowire and intrinsic high electrical conductivity for facile electron transport during Li^+ storage process. Our work offers a promising approach via a rational hybridization of two electrochemical energy storage materials for harvesting high capacity and good rate performance.

KEYWORDS: *titanium carbide, lithium storage mechanism, core/shell nanoarchitecture, lithium-ion batteries, metal oxides*

INTRODUCTION

Transition metal carbides (TMCs) have attracted increasing interest as cutting tools, reinforced components, machine parts, hard and anticorrosion coating owing to high melting point, high hardness, excellent chemical stability, and good electrical conductivity.[1−4] Moreover, some TMCs such as WC, TiC, TaC, etc. show similar sp electronic properties and catalytic performances with noble metals, so replacing Pt, Au, and Pd with TMCs can reduce the cost of catalysts significantly.[5] For example, tungsten carbide (WC) has been well-investigated as the catalyst support or the independent electrocatalyst for hydrogen evolution reaction,[6] hydrogen oxidation reaction,[7] methanol oxidation reaction,[8] and oxygen reduction reaction[9] over the past decades. Currently, titanium carbide (TiC) is of special interest owing to its unique properties including good electrical conductivity (6.8×10^{-5} Ω cm), low density (4.93 g cm^{-3}), and outstanding catalytic activity for CO and O_2 adsorption and dissociation.[10−13] There has been a growing endeavor in identifying potential applications in the fields of electrochemical energy storage and electrocatalysis.[14−17] Both theoretical and experimental results reveal that TiC shows the highest electrochemical stability among various TMCs thin films as the support for low-cost electrocatalysts.[18] In our previous work, the fine Pt nanoparticles supported on the TiC and NbC nanowires exhibit outstanding electrocatalytic performance toward methanol oxidation reaction, benefiting from superior chemical stability and good electrical conductivity.[4,19] TiC also presents high electrocatalytic activity for triiodide reduction as the counter electrode of dye-sensitized solar cells (DSSCs).[20] In terms of electrochemical energy storage, Lukatskaya and co-workers[21] pointed out "Mxenes" (Ti_2C, Ti_3C_2) titanium carbide exhibited superior lithium storage performance due to their low specific resistance. It has been demonstrated that some nanostructures, such as nanowires and core/shell hybrid nanowires, not only provide fast electron transport and short lithium diffusion path but also accommodate large volume changes and avoid rapid capacity fading during long-term cycling especially at high rates.[22−24] In

Received: February 11, 2015
Accepted: May 19, 2015
Published: May 19, 2015

DOI: 10.1021/acsami.5b01372
ACS Appl. Mater. Interfaces 2015, 7, 11842−11848

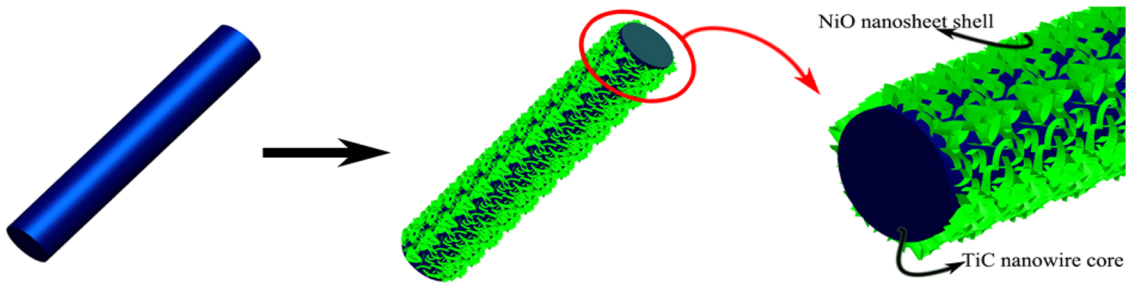

Figure 1. Schematic of TiC/NiO core/shell nanoarchitecture.

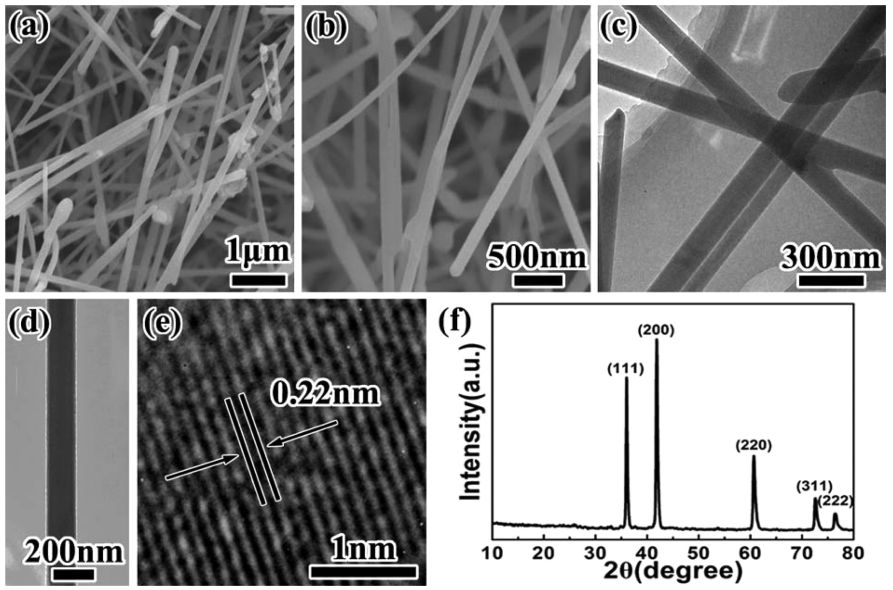

Figure 2. (a) Low- and (b) high-magnification SEM images of TiC nanowires. (c, d) TEM images of TiC nanowires and an individual nanowire. (e) HRTEM image of TiC nanowires. (f) XRD pattern of TiC nanowires.

our group, a series of TMC nanowires (TiC, NbC, TaC, SiC, B_4C, etc.) have been successfully fabricated by a biotemplated carbon-thermal method.[25−27] In our group, a series of TMC nanowires (TiC, NbC, TaC, SiC, B_4C etc.) were successfully synthesized by a facile biotemplated method.[25−27] Considering the merits of well-defined geometry, high electrochemical stability, and good electrical conductivity, TiC nanowires shows fascinating potential for lithium-ion batteries (LIBs). However, up to now, there are rare reports on TMCs nanowires as electrode materials for LIBs.

In recent years, transition metal oxides (NiO, Fe_2O_3, Fe_3O_4, CoO, Co_3O_4, MnO, Mn_3O_4, etc.) have been considered as promising alternative anode materials for LIBs because of higher theoretical capacity (718 mAh g^{-1} for NiO) than commercial carbon materials.[28−32] However, on account of poor electronic conductivity, large volume changes, and materials pulverization over extended cycling, the electrical connection of NiO with current collectors can be damaged, and the electrode integrity cannot be maintained well. As a result, most of the NiO materials show low capacity retention, poor rate performance, and slow kinetics of lithium ions and electron transport within electrodes. To address these issues, numerous efforts are devoted to the fabrication of various NiO nanostructures, for example, nanowire,[33] nanorod,[34,35] nanosheet,[36,37] or design of nanocomposite[28,38−40] to optimize and enhance their electrochemical performance.

Herein, a novel TiC/NiO core/shell nanoarchitecture (Figure 1) is designed as a promising anode material for LIBs, demonstrating an interesting battery-capacitive synchronous lithium storage mechanism. The TiC/NiO core/shell nanoarchitecture offers high specific capacity, good capacity retention, and remarkable rate capability, which can be ascribed to the double-layer capacitive characteristics of TiC nanowire and the intrinsic high electrical conductivity for facile electron transport during Li^+ storage process.

EXPERIMENTAL SECTION

Synthesis of TiC Nanowires. As previously reported in our work, TiC nanowires were synthesized by a simple, convenient, and cost-effective biotemplated method using cotton T-shirts as the carbon source and the template.[19,27] To remove unwanted elements such as Ni, Na, Cl, etc. derived from the reagents, the acquired sample was immersed into a mixed solution of 50 mL of hydrochloric acid and 150 mL of deionized water for 0.5 h at room temperature. Finally, the TiC nanowires were washed by deionized water and dried at 80 °C overnight.

Synthesis of TiC/NiO Core/Shell Nanoarchitecture. First, 0.1 g of TiC nanowires and 0.436 g of $Ni(NO_3)_2{\cdot}6H_2O$ were put into 50 mL of solution of isopropyl alcohol and deionized water (1:1 by volume) with ultrasound treatment for 1 h. Subsequently, 4 mL of ammonia solution ($NH_3{\cdot}H_2O$, 25 wt %) was added into the above suspension slowly. After it was stirred continuously by magnetic stirring for 1 h, the suspension was transferred into a 100 mL Teflon-lined stainless steel autoclave, heated at 180 °C for 8 h, and then cooled to room temperature naturally. The precursor precipitate was

DOI: 10.1021/acsami.5b01372
ACS Appl. Mater. Interfaces 2015, 7, 11842−11848

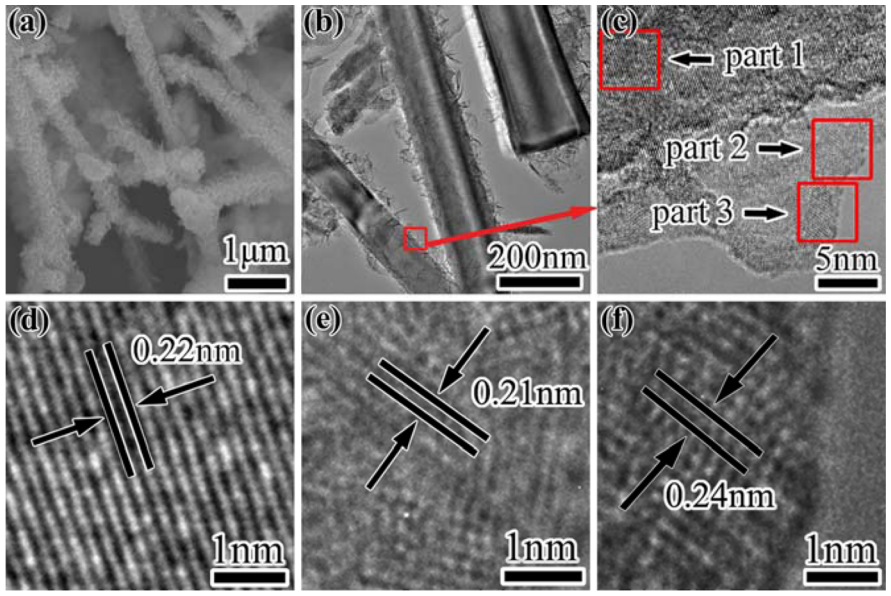

Figure 3. (a) SEM and (b) TEM images of TiC/NiO core/shell nanoarchitecture. (c) HRTEM image of the square area in b. (d–f) Magnified HRTEM images of the square areas named part 1, 2, and 3, respectively, in (c).

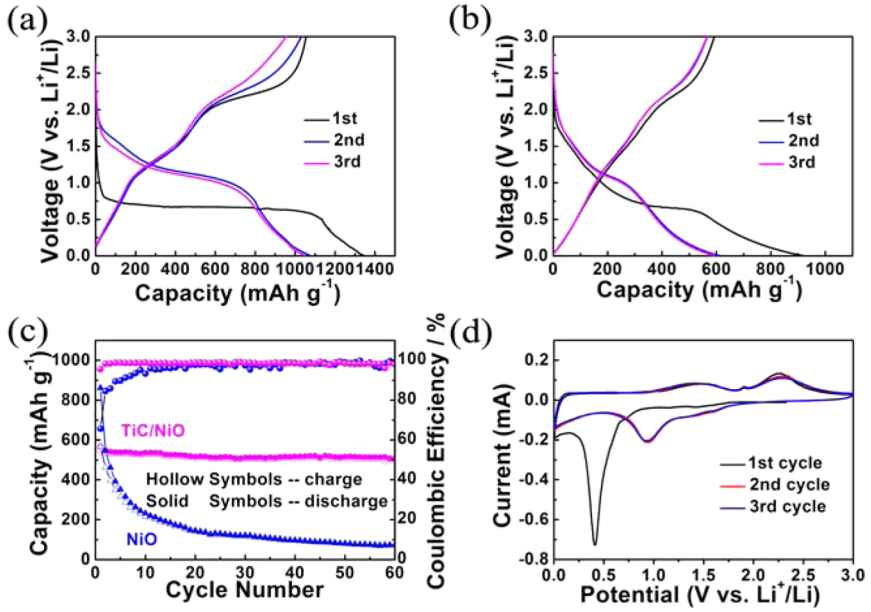

Figure 4. Initial charge/discharge profiles of (a) NiO and (b) TiC/NiO core/shell nanoarchitecture at 50 mA g^{-1}. (c) Cycling stability and Coulombic efficiency of the NiO and TiC/NiO core/shell nanoarchitecture at 200 mA g^{-1}. (d) CVs of TiC/NiO core/shell nanoarchitecture at 0.1 mV s^{-1}.

centrifuged and washed with deionized water and ethanol, and dried at 80 °C for 12 h. Finally, the precursor was annealed at 350 °C for 3 h under nitrogen atmosphere to obtain TiC/NiO core/shell nanowires. The mass percent of NiO in the nanocomposite was determined by measuring the sample before and after the NiO deposition on a microbalance (Mettler Toledo AL104, 0.1 μg of resolution). For comparison, pure NiO was also prepared by a similar process as that for the TiC/NiO core/shell nanoarchitecture but without adding TiC nanowires.

Characterization. X-ray diffraction (XRD) analysis of the samples was conducted on an Rigaku Ultima IV diffractometer with a Cu Kα radiation. The morphology and microstructure was characterized by scanning electron microscope (SEM, Hitachi S-4800) and transmission electron microscope (TEM, FEI Tecnai G^2 F30). Nitrogen adsorption–desorption was evaluated by Brunauer–Emmett–Teller (BET) tests with an ASAP 2020 surface area and pore analyzers (Micromeritics Instruments).

Electrochemical Measurements. CR2025-type coin cells were assembled and used to evaluate the electrochemical performance of as-synthesized materials. The test electrode consisted of as-synthesized material, Super-P, and polyvinylidene fluoride (PVDF) binder with the weight ratio of 70:20:10. The test electrode was prepared by casting the slurry onto a copper foil and drying in a vacuum oven at 120 °C overnight. A lithium foil was used as the counter and the reference electrodes. The electrolyte was a solution of 1 M $LiPF_6$ dissolved in dimethyl carbonate(DMC)/ethylene carbonate(EC) (1:1 by volume), while Cellgard 2300 polypropylene microporous film was selected as the separator. The charge and discharge tests were operated on a Shenzhen Neware battery testing instrument in the voltage range of 0.005–3.0 V (vs Li/Li^+). Cyclic voltammetry (CV) was performed on

DOI: 10.1021/acsami.5b01372
ACS Appl. Mater. Interfaces 2015, 7, 11842–11848

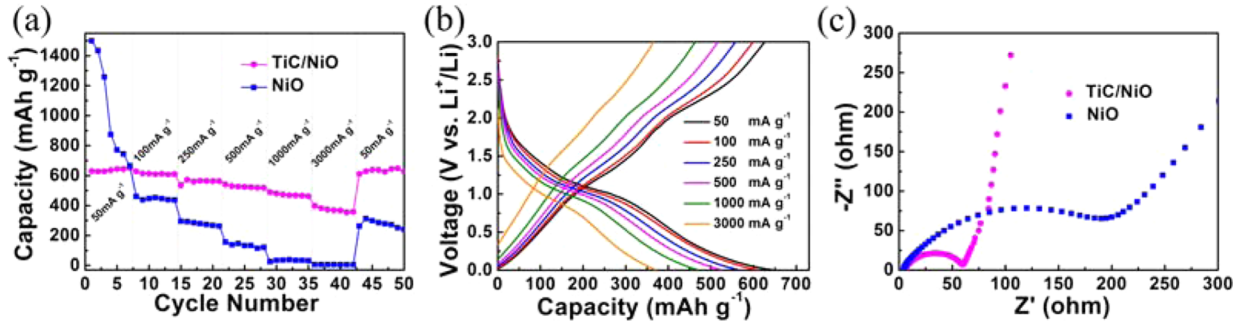

Figure 5. (a) Rate performance of NiO and TiC/NiO core/shell nanoarchitecture. (b) Representative discharge/charge profiles at various current densities. (c) Nyquist plots of NiO and TiC/NiO electrodes.

a CHI660D electrochemical instrument at various scanning rates of 0.10, 0.25, 0.50, 0.75, 1.00 mV s^{-1}, respectively. Electrochemical impedance spectroscopy (EIS) was measured in the frequency range from 100 kHz to 0.01 Hz.

RESULTS AND DISCUSSION

Figure 2a,b displays the SEM images of TiC nanowires. The as-obtained product contains a great number of homogeneous nanowires, exhibiting highly oriented growth characteristics. The diameter is in the range of 100−150 nm, and the length is up to several micrometers. The TEM images of TiC nanowires (Figure 2c) and an individual nanowire (Figure 2d) were taken to display detailed morphological characteristics. It appears that the surfaces of the nanowires are clear and smooth. In the HRTEM image of the TiC nanowire (Figure 2e), the spacing between the adjacent lattice fringes is ∼0.22 nm, which corresponds to (200) planes of cubic TiC. Figure 2f shows the XRD pattern of TiC nanowires. All the intense peaks are well-matched with cubic TiC (*Fm*3*m*) (JCPDS No. 65-8807). The reflections at 36.0°, 41.8°, 60.7°, 72.6°, 76.4° can be indexed to (111), (200), (220), (311), and (222) crystal planes, respectively. Ti metal, TiO_xC_y and Ti_xO_y phases were not detected, suggesting that TiO_2 has been converted into TiC and that the product purity is extremely high.

Figure 3a represents an SEM image of TiC/NiO core/shell nanoarchitecture. It can be seen that the NiO shell is composed of many interconnected NiO nanosheets. These nanosheets grow on the TiC nanowires, forming a three-dimensional porous structure. Generally, a highly porous structure facilitates electrolyte transportation and Li^+ diffusion and also accommodates the volume change associated with Li^+ insertion and extraction. However, pure NiO sample synthesized by the same method exhibits a flowerlike structure, which is assembled by nanosheets (Supporting Information, Figure S1a,b). Figure 3c is taken from the edge area of a TiC/NiO nanowire in Figure 3b. The NiO nanosheets are connected well to the TiC nanowires substrate so that all the nanosheets contribute to the capacity. Figure 3d−f presents the magnified HRTEM images of the marked regions in Figure 3c. The adjacent lattice fringes with an interplanar spacing of 0.22 nm corresponds to the (200) crystal planes of cubic TiC, while 0.21 and 0.24 nm are assigned to the (200) and (111) crystal planes of cubic NiO, respectively, which are also matching well with the XRD pattern of TiC/NiO in Supporting Information, Figure S2.

To study the lithium storage properties of the as-synthesized samples, a series of electrochemical measurements were conducted at room temperature. All the specific capacities are calculated based on the total mass of the samples. Figure 4a shows the initial charge/discharge profiles of the NiO electrode at 50 mA g^{-1}. A long and flat voltage plateau appears at ∼0.70 V during the first discharge process. From the second cycle onward, the discharge plateaus shifts to ∼1.0 V. The NiO electrode displays a high discharge capacity of 1344.4 mAh g^{-1} in the first cycle and drops to 1047.9 mAh g^{-1} in the third cycle. For the TiC/NiO core/shell nanoarchitecture, the first discharge capacity is only 918.1 mAh g^{-1}; however, better capacity retention is demonstrated by good overlap of the charge and discharge curves upon cycling. After the sample was activated at 50 mA g^{-1} for three cycles, the cycling stability and Coulombic efficiency of the NiO and TiC/NiO core/shell nanoarchitecture were measured at 200 mA g^{-1}. In Figure 4c, the specific capacities of TiC/NiO core/shell nanoarchitecture are higher than that of the NiO electrode except the first discharging. More importantly, the TiC/NiO electrode demonstrates much better cycling stability with a slight capacity fade from 568.1 to 507.5 mAh g^{-1} during 60 cycles (90% capacity retention). By contrast, the discharge capacity of the NiO electrode drops sharply to 79.6 mAh g^{-1} by cycle 60. The superior capacity retention of the TiC/NiO core/shell nanoarchitecture can be ascribed to its novel configuration and high porous structure. First, the voids among NiO nanosheets provide enough spaces to accommodate and mitigate the volume change. Second, TiC nanowires have excellent chemical and electrochemical stability, maintaining the nanowire integrity well during repeated cycling.

It should be mentioned that the TiC/NiO core/shell nanoarchitecture has a higher reversible capacity than the calculated theoretical value. The mass percent of NiO in the composite is ∼32 wt %, determined by measuring the sample before and after the deposition. Thus, the theoretical value of the TiC/NiO (32 wt %) composite can be calculated as ∼348.8 mAh g^{-1} based on the theoretical capacity of NiO (718 mAh g^{-1}) and actual capacity of TiC nanowires (175 mAh g^{-1}) at 200 mA g^{-1} in Supporting Information, Figure S3. Figure 4c clearly indicates that the actual capacity of the TiC/NiO composite keeps above 507.5 mAh g^{-1} throughout the cycling process. This is an abnormal phenomenon for metal oxide anode material. Very interestingly, our work indicates that the TiC electrode shows obvious double-layer capacitor behavior, which is confirmed by both CV and EIS measurements. As shown in Supporting Information, Figure S4, the CV curves are nearly rectangular in the potential range of 0.25−1.25 V, demonstrating good charge propagation in the TiC electrode. At a high scan rate of 1.0 mV s^{-1}, the CV curves show slight variance, indicating a characteristic of electrochemical double-layer capacitor. Supporting Information, Figure S5 shows the

DOI: 10.1021/acsami.5b01372
ACS Appl. Mater. Interfaces 2015, 7, 11842−11848

EIS of TiC electrode. The plots at low frequencies are almost dispersed along a vertical line, which is similar to that of an ideal double-layer capacitor. Figure 4d shows the CV curves of the TiC/NiO electrode at 0.1 mV s^{-1}. A strong reduction peak is observed at 0.41 V in the first cathodic scanning, which corresponds to the conversion of NiO into Ni ($NiO + 2Li \rightarrow Ni + Li_2O$), the formation of amorphous Li_2O, and solid electrolyte interface (SEI). Because of the drastic lithium driven, textural, or structural modifications, this reduction peak moves to 0.93 V in the subsequent scanning. The good overlap of the CV profiles indicates the good stability and reversibility of the electrode. Besides redox peaks of NiO, there is a higher background current in the CV curves of the TiC/NiO electrode than that of the TiC electrode (Figure S4), implying the TiC/NiO electrode has a higher specific capacitance than the TiC electrode. The enhanced capacitive effect can be ascribed to the large electrode/electrolyte contact area of porous nanoarchitecture and to the rational combination of two energy storage materials. Supporting Information, Figure S6 confirms that the TiC/NiO core/shell nanoarchitecture show higher BET surface area than the TiC nanowires. On the basis of these results, it can be inferred that the high specific capacity delivered by the TiC/NiO electrode originates from synchronous battery-capacitive energy storage system.

The rate performance of the NiO and TiC/NiO core/shell nanoarchitecture electrodes at various current rates (increase stepwise from 50 to 3000 mA g^{-1} and finally return to 50 mA g^{-1}) are presented in Figure 5a. The discharge capacity of the TiC/NiO core/shell nanoarchitecture decreases gradually with increasing the current rate. A satisfactory capacity of 367.6 mAh g^{-1} is obtained even at a high rate of 3000 mA g^{-1}. As for this capacity, the portion derived from NiO is calculated to be ~770 mAh g^{-1}, which is comparable with the previously reported values for NiO, such as mesoporous NiO microspheres[41] delivering a capacity of 621 mAh g^{-1} at 1000 mA g^{-1}, NiO nanosheets/graphene composite[29] achieving a reversible capacity of 550 mAh g^{-1} at 2.5 A g^{-1}, and pollen-templated NiO/C[42] with a capacity of 352 mAh g^{-1} at 3 A g^{-1}. When the current density returns to 50 mA g^{-1}, this material can recover the initial capacity and even surpass it. By comparison, the discharge capacity of NiO drops dramatically as the current density increases from 50 to 3000 mA g^{-1}. Figure 5a clearly demonstrates that the rate capability of the TiC/NiO electrode is much better as compared to the NiO electrode.

To further clarify the battery-capacitive energy storage mechanism of the TiC/NiO electrode, the representative discharge/charge profiles at various current densities are displayed in Figure 5b. The discharge capacities at 50, 100, 250, 500, 1000, and 3000 mA g^{-1} are 635.6, 609.0, 564.3, 523.8, 468.6, and 369.4 mAh g^{-1}, respectively. It is noteworthy that, at a low rate of 50 and 100 mA g^{-1}, two charge plateaus and one discharge plateau can be identified, somewhat similar to that of NiO. With increasing the current density, however, these voltage plateaus gradually become vague. At a high rate of 3000 mA g^{-1}, the charge/discharge curves are nearly inclined in shape with good symmetry, exhibiting a typical characteristic of double-layer capacitor. The outstanding rate capability suggests fast and facile electron/ion transport due to its capacitive energy storage mechanism.

Figure 5c shows the Nyquist plots of fresh NiO and TiC/NiO core/shell nanoarchitecture electrodes, which were measured in a frequency range between 0.01 Hz and 100 kHz. The EIS of NiO electrode is composed of a depressed semicircle in the high-frequency zone and a sloping line in the low-frequency zone. The semicircle is attributed to the charge-transfer resistance on the electrode/electrolyte interface; the sloping line is called the Warburg resistance, representing Li^+ diffusion kinetics in the electrode. Obviously, the semicircle size of the TiC/NiO electrode is much smaller than the NiO electrode, indicating that the electron/ion transport on the electrode/electrolyte interface is strikingly enhanced. This may be related to the good electrical conductivity of TiC nanowires and increased electrode/electrolyte contact area owing to the core/shell nanoarchitecture. Furthermore, the low-frequency line of the TiC/NiO electrode displays a large slope (~90°), which closely corresponds to an ideal capacitor. Such an steep line is a symbol of high Li-ion diffusion rate in the electrode. Therefore, it can be concluded that these combined merits of low charge-transfer resistance, fast Li-ion diffusion rate, and extraordinary double-layer capacitor behavior lead to outstanding rate performance of TiC/NiO core/shell nanoarchitecture.

CONCLUSIONS

In summary, a novel TiC/NiO core/shell nanoarchitecture has been fabricated, demonstrating a battery-capacitive synchronous Li storage mechanism. The TiC/NiO electrode offers high overall capacity and excellent rate capability. The reversible capacity reaches 568.1 mAh g^{-1} at 200 mA g^{-1} with the capacity retention of 90% after 60 cycles. It can still deliver a satisfactory capacity of 367.6 mAh g^{-1} even at 3000 mA g^{-1}. The sparking results can be attributed to the facile electron/ionic transport and the improved reaction kinetics resulting from the core/shell nanoarchitecture and the combination of two energy storage materials. Moreover, the obvious double-layer capacitive and high electrical conductivity of the TiC nanowire core have also made a great contribution to the outstanding electrochemical performance.

ASSOCIATED CONTENT

Supporting Information

Additional experimental data including SEM of pure NiO, XRD of pure NiO and TiC/NiO core/shell nanoarchitecture, cycling performance, cyclic voltammograms and Nyquist plots of TiC nanowires, nitrogen adsorption−desorption isotherms of TiC/NiO core/shell nanoarchitecture and TiC nanowires. The Supporting Information is available free of charge on the ACS Publications website at DOI: 10.1021/acsami.5b01372.

AUTHOR INFORMATION

Corresponding Authors

*Phone/Fax: +86 571 88320394. E-mail: msechem@zjut.edu.cn. (W.K.Z.)

*E-mail: tao@zjut.edu.cn. (X.T.)

Notes

The authors declare no competing financial interest.

ACKNOWLEDGMENTS

The authors appreciate the support from National Natural Science Foundation of China (201403196, 51201151, 51172205), Natural Science Foundation of Zhejiang Province (LR13E020002 and LY13E020010), Visiting Scholar Foundation from State Key Lab of Silicon Materials, Zhejiang University (SKL2014-2), Scientific Research Foundation of Zhejiang Provincial Education Department (Y201432424).

DOI: 10.1021/acsami.5b01372
ACS Appl. Mater. Interfaces 2015, 7, 11842−11848

REFERENCES

(1) Naguib, M.; Halim, J.; Lu, J.; Cook, K. M.; Hultman, L.; Gogotsi, Y.; Barsoum, M. W. New Two-Dimensional Niobium and Vanadium Carbides as Promising Materials for Li-Ion Batteries. *J. Am. Chem. Soc.* **2013**, *135*, 15966−15969.

(2) Hunt, S. T.; Nimmanwudipong, T.; Román-Leshkov, Y. Engineering Non-Sintered, Metal-Terminated Tungsten Carbide Nanoparticles for Catalysis. *Angew. Chem., Int. Ed.* **2014**, *53*, 5131−5136.

(3) Liu, Y.; Kelly, T. G.; Chen, J. G.; Mustain, W. E. Metal Carbides as Alternative Electrocatalyst Supports. *ACS Catal.* **2013**, *3*, 1184−1194.

(4) Qiu, Z.; Huang, H.; Du, J.; Feng, T.; Zhang, W. K.; Gan, Y. P.; Tao, X. Y. NbC Nanowire-Supported Pt Nanoparticles as a High Performance Catalyst for Methanol Electrooxidation. *J. Phys. Chem. C* **2013**, *117*, 13770−13775.

(5) Kelly, T. G.; Chen, J. G. Metal Overlayer on Metal Carbide Substrate: Unique Bimetallic Properties for Catalysis and Electrocatalysis. *Chem. Soc. Rev.* **2012**, *41*, 8021−8034.

(6) Chen, W. F.; Muckerman, J. T.; Fujita, E. Recent Developments in Transition Metal Carbides and Nitrides as Hydrogen Evolution Electrocatalysts. *Chem. Commun.* **2013**, *49*, 8896−8909.

(7) Hara, Y.; Minami, N.; Matsumoto, H.; Itagaki, H. New Synthesis of Tungsten Carbide Particles and the Synergistic Effect with Pt Metal as a Hydrogen Oxidation Catalyst for Fuel Cell Applications. *Appl. Catal., A* **2007**, *332*, 289−296.

(8) Erich, C. W.; Alan, L. S.; Michael, B. Z.; Chen, J. G. Tungsten Monocarbide as Potential Replacement of Platinum for Methanol Electrooxidation. *J. Phys. Chem. C* **2007**, *40*, 14617−14620.

(9) Hsu, I. J.; Hansgen, D. A.; McCandless, B. E.; Willis, B. G.; Chen, J. G. Atomic Layer Deposition of Pt on Tungsten Monocarbide (WC) for the Oxygen Reduction Reaction. *J. Phys. Chem. C* **2011**, *115*, 3709−3715.

(10) Zou, G. F.; Wang, H. Y.; Nathan, M.; Luo, H. M.; Nan, L.; Di, Z. F.; Eve, B.; Wang, Y. Q.; Thomas, M.; Anthony, B.; Zhang, X. H.; Michael, N.; Jia, Q. X. Chemical Solution Deposition of Epitaxial Carbide Films. *J. Am. Chem. Soc.* **2010**, *132*, 2516−2517.

(11) Huang, C. H.; Gu, D.; Zhao, D. Y.; Doong, R. A. Direct Synthesis of Controllable Microstructures of Thermally Stable and Ordered Mesoporous Crystalline Titanium Oxides and Carbide/Carbon Composites. *Chem. Mater.* **2010**, *22*, 1760−1767.

(12) Rodríguez, J. A.; Feria, L.; Jirsak, T.; Takahashi, Y.; Nakamura, K.; Illas, F. Role of Au-C Interactions on the Catalytic Activity of Au Nanoparticles Supported on TiC(001) toward Molecular Oxygen Dissociation. *J. Am. Chem. Soc.* **2010**, *132*, 3177−3186.

(13) Rodriguez, J. A.; Liu, P.; Viñes, F.; Illas, F.; Takahashi, Y.; Nakamura, K. Dissociation of SO_2 on Au/TiC(001): Effects of Au-C Interactions and Charge Polarization. *Angew. Chem., Int. Ed.* **2008**, *120*, 6787−6791.

(14) Yu, X.; Zhao, X. A.; Liu, Y. Y.; Hua, M.; Jiang, X. The Effects of Ti Carbonization on the Nucleation and Oriented Growth of Diamond Films on Cemented Carbide. *ACS Appl. Mater. Interfaces* **2014**, *6*, 4669−4677.

(15) Esposito, D. V.; Hunt, S. T.; Kimmel, Y. C.; Chen, J. G. A New Class of Electrocatalysts for Hydrogen Production from Water Electrolysis: Metal Monolayers Supported on Low-Cost Transition Metal Carbides. *J. Am. Chem. Soc.* **2012**, *134*, 3025−3033.

(16) Flaherty, D. W.; May, R. A.; Berglund, S. P.; Stevenson, K. J.; Mullins, C. B. Low Temperature Synthesis and Characterization of Nanocrystalline Titanium Carbide with Tunable Porous Architectures. *Chem. Mater.* **2010**, *22*, 319−329.

(17) Grove, D. E.; Gupta, U.; Castleman, A. W., Jr. Effect of Carbon Concentration on Changing the Morphology of Titanium Carbide Nanoparticles from Cubic to Cuboctahedron. *ACS Nano* **2010**, *4*, 49−54.

(18) Kimmel, Y. C.; Xu, X. G.; Yu, W. T.; Yang, X. D.; Chen, J. G. Trends in Electrochemical Stability of Transition Metal Carbides and Their Potential Use As Supports for Low-Cost Electrocatalysts. *ACS Catal.* **2014**, *4*, 1558−1562.

(19) Qiu, Z.; Huang, H.; Du, J.; Tao, X. Y.; Xia, Y.; Feng, T.; Gan, Y. P.; Zhang, W. K. Biotemplated Synthesis of Bark-Structured TiC Nanowires as Pt Catalyst Supports with Enhanced Electrocatalytic Activity and Durability for Methanol Oxidation. *J. Mater. Chem. A* **2014**, *2*, 8003−8009.

(20) Wu, M. X.; Lin, X.; Wang, Y. D.; Wang, L.; Guo, W.; Qi, D. D.; Peng, X. J.; Hagfeldt, A.; Grätzel, M.; Ma, T. L. Economical Pt-Free Catalysts for Counter Electrodes of Dye-Sensitized Solar Cells. *J. Am. Chem. Soc.* **2012**, *134*, 3419−3428.

(21) Lukatskaya, M. R.; Mashtalir, O.; Ren, C. E.; Dall'Agnese, Y.; Rozier, P.; Taberna, P. L.; Naguib, M.; Simon, P.; Barsoum, M. W.; Gogotsi, Y. Cation Intercalation and High Volumetric Capacitance of Two-Dimensional Titanium Carbide. *Science* **2013**, *341*, 1502−1507.

(22) Yao, Y.; Huo, K. F.; Hu, L. B.; Liu, N.; Judy, J. C.; Matthew, T. M.; Paul, K. C.; Cui, Y. Highly Conductive, Mechanically Robust, and Electrochemically Inactive TiC/C Nanofiber Scaffold for High-Performance Silicon Anode Batteries. *ACS Nano* **2011**, *5*, 8346−8351.

(23) Cheng, K.; Yang, F.; Ye, K.; Zhang, Y.; Jiang, X.; Yin, J. L.; Wang, G. L.; Cao, D. X. Highly Porous Fe_3O_4-Fe Nanowires Grown on C/TiC Nanofiber Arrays as the High Performance Anode of Lithium-Ion Batteries. *J. Power Sources* **2014**, *258*, 260−265.

(24) Szczech, J. R.; Jin, S. Nanostructured Silicon for High Capacity Lithium Battery Anodes. *Energy Environ. Sci.* **2011**, *4*, 56−72.

(25) Tao, X. Y.; Dong, L. X.; Wang, X. N.; Zhang, W. K.; Nelson, B. J.; Li, X. D. B_4C-Nanowires/Carbon-Microfiber Hybrid Structures and Composites from Cotton T-shirts. *Adv. Mater.* **2010**, *22*, 2055−2059.

(26) Tao, X. Y.; Du, J.; Li, Y. P.; Yang, Y. C.; Fan, Z.; Gan, Y. P.; Huang, H.; Zhang, W. K.; Dong, L. X.; Li, X. D. TaC Nanowire/Activated Carbon Microfiber Hybrid Structures from Bamboo Fibers. *Adv. Energy Mater.* **2011**, *1*, 534−539.

(27) Tao, X. Y.; Du, J.; Yang, Y. C.; Li, Y. P.; Xia, Y.; Gan, Y. P.; Huang, H.; Zhang, W. K.; Li, X. D. TiC Nanorods Derived from Cotton Fibers: Chloride-Assisted VLS Growth, Structure, and Mechanical Properties. *Cryst. Growth Des.* **2011**, *11*, 4422−4426.

(28) Xia, X. H.; Zeng, Z. Y.; Li, X. L.; Zhang, Y. Q.; Tu, J. P.; Fan, N. C.; Hua, Z.; Fan, H. J. Fabrication of Metal Oxide Nanobranches on Atomic-Layer-Deposited TiO_2 Nanotube Arrays and Their Application in Energy Storage. *Nanoscale* **2013**, *5*, 6040−6047.

(29) Zhou, G. M.; Wang, D. W.; Yin, L. C.; Li, N.; Li, F.; Ming, C. H. Oxygen Bridges between NiO Nanosheets and Graphene for Improvement of Lithium Storage. *ACS Nano* **2012**, *6*, 3214−3223.

(30) Huang, Y.; Huang, X. L.; Lian, J. S.; Xu, D.; Wang, L. M.; Zhang, X. B. Self-Assembly of Ultrathin Porous NiO Nanosheets/Graphene Hierarchical Structure for High-Capacity and High-Rate Lithium Storage. *J. Mater. Chem.* **2012**, *22*, 2844−2847.

(31) Sun, X. L.; Si, W. P.; Liu, X. H.; Deng, J. W.; Xi, L. X.; Liu, L. F.; Yan, C. L.; Schmidt, O. G. Multifunctional Ni/NiO Hybrid Nanomembranes as Anode Materials for High-Rate Li-Ion Batteries. *Nano Energy* **2014**, *9*, 168−175.

(32) Lai, L. F.; Zhu, J. X.; Li, Z. G.; Yu, D. Y. W.; Jiang, S. R.; Cai, X. Y.; Yan, Q. Y.; Lam, Y. M.; Shen, Z. X.; Lin, J. Y. Co_3O_4/Nitrogen Modified Graphene Electrode as Li-Ion Battery Anode with High Reversible Capacity and Improved Initial Cycle Performance. *Nano Energy* **2014**, *3*, 134−143.

(33) Wei, Z. P.; Arredondo, M.; Peng, H. Y.; Zhang, Z.; Guo, D. L.; Xing, G. Z.; Li, Y. F.; Wong, L. M.; Wang, S. J.; Valanoor, N.; Wu, T. A Template and Catalyst-Free Metal Etching-Oxidation Method to Synthesize Aligned Oxide Nanowire Arrays: NiO as an Example. *ACS Nano* **2010**, *4*, 4785−4791.

(34) Lu, Z. Y.; Chang, Z.; Liu, J. F.; Sun, X. M. Stable Ultrahigh Specific Capacitance of NiO Nanorod Arrays. *Nano Res.* **2011**, *4*, 658−665.

(35) Bai, Z. C.; Zhang, X. Y.; Zhang, Y. W.; Guo, C. L.; Tang, B. Facile Synthesis of Mesoporous Mn_3O_4 Nanorods as a Promising Anode Material for High Performance Lithium-Ion Batteries. *J. Mater. Chem. A* **2014**, *2*, 16755−16760.

(36) Zhang, G. Q.; Yu, L.; Hoster, H. E.; Lou, X. W. Synthesis of One-Dimensional Hierarchical NiO Hollow Nanostructures with Enhanced Supercapacitive Performance. *Nanoscale* **2013**, *5*, 877−881.

DOI: 10.1021/acsami.5b01372
ACS Appl. Mater. Interfaces 2015, 7, 11842−11848

(37) Vijayakumar, S.; Nagamuthu, S.; Muralidharan, G. Supercapacitor Studies on NiO Nanoflakes Synthesized Through a Microwave Route. *ACS Appl. Mater. Interfaces* **2013**, *5*, 2188−2196.
(38) Gao, X. P.; Yang, H. X. Multi-Electron Reaction Materials for High Energy Density Batteries. *Energy Environ. Sci.* **2010**, *3*, 174−189.
(39) Xia, X. H.; Tu, J. P.; Zhang, Y. Q.; Wang, X. L.; Gu, C. D.; Zhao, X. B.; Fan, H. J. High-Quality Metal Oxide Core/Shell Nanowire Arrays on Conductive Substrates for Electrochemical Energy Storage. *ACS Nano* **2012**, *6*, 5531−5538.
(40) Xiong, Q. Q.; Xia, X. H.; Tu, J. P.; Chen, J.; Zhang, Y. Q.; Zhou, D.; Gu, C. D.; Wang, X. L. Hierarchical Fe_2O_3@Co_3O_4 Nanowire Array Anode for High-Performance Lithium-Ion Batteries. *J. Power Sources* **2013**, *240*, 344−350.
(41) Bai, Z. C.; Ju, Z. C.; Guo, C. L.; Qian, Y. T.; Tang, B.; Xiong, S. L. Direct Large-Scale Synthesis of 3D Hierarchical Mesoporous NiO Microspheres as Highperformance Anode Materials for Lithium Ion Batteries. *Nanoscale* **2014**, *6*, 3268−3273.
(42) Xia, Y.; Zhang, W. K.; Xiao, Z.; Huang, H.; Zeng, H. J.; Chen, X. R.; Chen, F.; Gan, Y. P.; Tao, X. Y. Biotemplated Fabrication of Hierarchically Porous NiO/C Composite from Lotus Pollen Grains for Lithium-Ion Batteries. *J. Mater. Chem.* **2012**, *22*, 9209−9215.

DOI: 10.1021/acsami.5b01372
ACS Appl. Mater. Interfaces 2015, 7, 11842−11848